Flocking Transitions in Confluent Tissues

F. Giavazzi, M. Paoluzzi, M. Macchi, D. Bi, G. Scita, M. L. Manning, R. Cerbino and M. C. Marchetti

1. Model simulation details

We performed numerical simulations by integrating the equations of motion with an Euler method for $N_t = 2^{17} - 2^{22}$ steps with integration time step $\Delta t = 10^{-2}$. The phase diagram was investigated performing $N_J \times N_p$ simulations, $N_J = 22$ with $J \in [0, 8]$ and $N_{p_0} = 32$, $p_0 \in [2.9, 4.1]$. The robustness of our results against finite size effects was evaluated by considering different systems sizes, namely $N = 100, 256, 400, 900, 1600, 3200, 4900$.

The phase diagram has been investigated considering a tissue composed of $N = 400$ cells. The nature of the flocking transition has been addressed studying the finite size effects on a system composed for $N = 100, 400, 1600, 3200$. To study the morphology of dynamical heterogeneities, we performed simulations of $N = 4900$ cells close to the solid/liquid transition. Both dynamical and structural properties of the system have been computed by sampling steady state trajectories. The steady state condition has been checked looking at the time evolution of the instantaneous Vicsek order parameter $\varphi(t)$ and cellular shape index $q(t)$ at time t. The system is considered to be at steady state when $\varphi(t)$ and $q(t)$ fluctuate around well-defined values. Dynamical observables and static properties have been computed by averaging over steady state trajectories in the time window $[0, T]$, where $t = 0$ denotes the beginning of the steady state regime as defined above and $t = T$ the end of the simulation. For example, the mean-square displacement $MSD(t)$ is explicitly calculated as

$$MSD(t) = \frac{1}{N(T-t)} \int_0^{T-t} dt_0 \sum_{i=1}^{N} [\mathbf{r}_i'(t+t_0) - \mathbf{r}_i'(t_0)]^2, \quad [1]$$

and the Vicsek order parameter as

$$\varphi = \frac{1}{NT} \int_0^{T} dt_0 \left| \sum_{i=1}^{N} \frac{\mathbf{v}_i(t_0)}{|\mathbf{v}_i(t_0)|} \right| . \quad [2]$$

In the above expressions, the time integral is numerically evaluated as a Riemann sum based on a partition of step Δt.

2. Mean square displacement in the solid phases

In the solid we model each cell i caged by its neighbors as a point particle tethered to a spring of elastic constant k. Considering first the isotropic solid, the dynamics of the fluctuations $\delta\mathbf{r}_i = \mathbf{r}_i - \mathbf{r}_i^0$ of a caged particle around its mean position, $\mathbf{r}_i^0$, is goiverned by the equations

$$\begin{aligned} \delta\dot{\mathbf{r}}_i &= v_0 \mathbf{n}_i - \mu k \delta\mathbf{r}_i \, , \quad [3] \\ \dot{\theta}_i &= \eta_i \, . \end{aligned}$$

The mean square displacement can be calculated analytically [57], with the result

$$MSD(t) = \frac{v_0^2}{2\mu k D_r} \frac{1 - e^{-\mu k t} - \frac{\mu k}{D_r}\left(1 - e^{-D_r t}\right)}{1 - (\frac{\mu k}{D_r})^2} \, , \quad [4]$$

and the long-time limit

$$\lim_{t\to\infty} MSD(t) = \frac{v_0^2}{\mu k(\mu k + D_r)} \, . \quad [5]$$

We now want to examine the mean-square displacement deep into the solid flocking state, in the limit large $J \gg D_r$. We model again an individual cell as a particle tethered to a spring of force constant k due to caging from the neighbors, but also moving at the mean velocity $\bar{\mathbf{v}} = \bar{v}(\cos\bar{\phi}, \sin\bar{\phi})$ of the flock. We orient the x axis along the direction of mean migration, corresponding to $\bar{\phi} = 0$, and let $\mathbf{v}_i = \bar{\mathbf{v}} + \delta\mathbf{v}_i$, with $\delta\mathbf{v}_i = (\dot{x}_i, \dot{y}_i)$, and $\dot{x}_i \simeq \delta v$ and $\dot{y}_i \simeq \bar{v}\phi_i$. Letting $\mathbf{e}_i \simeq (1, \theta_i)$, the equations of motion for the fluctuations are

$$\begin{aligned} \dot{x}_i &= v_0 - \mu k x_i \, , \quad [6] \\ \dot{y}_i &= v_0 \theta_i - \mu k y_i \, , \quad [7] \\ \dot{\theta}_i &= -J\left(\theta_i - \frac{\dot{y}_i}{\bar{v}}\right) + \eta_i \, . \quad [8] \end{aligned}$$

Fluctuations transverse and logitudinal to the direction of mean motion are decoupled. Eliminating the angular dynamics in favor of y_i, Eqs. Eq. (7) and Eq. (8) can be recast in the form of a second order differential equation for y_i. At long times this reduces to

$$\dot{y}_i = -\frac{J\mu k y_i}{\mu k + J\left(1 - \frac{v}{v_0}\right)} + \frac{v_0 \eta_i}{\mu k + J\left(1 - \frac{v}{v_0}\right)} \, . \quad [9]$$

The transverse part of the mean-square displacement can then be immediately obtained as

$$\langle [y_i(t)]^2 \rangle = \frac{v_0^2 D_r}{J\mu k \left[\mu k + J\left(1 - \frac{v}{v_0}\right)\right]} \left(1 - e^{-\frac{J\mu k}{\mu k + J(1-\frac{v}{v_0})} t}\right) , \quad [10]$$

with long-time limit

$$\lim_{t\to\infty} \langle [y_i(t)]^2 \rangle = \frac{v_0^2 D_r}{J\mu k \left[\mu k + J\left(1 - \frac{v}{v_0}\right)\right]} . \quad [11]$$

Deep in the flocking state we can approximate $\bar{v} \sim v_0$ and identify $T_{eff} = v_0^2 D_r / J\mu^2 k$.

3. Finite-size effects and nature of the flocking transition

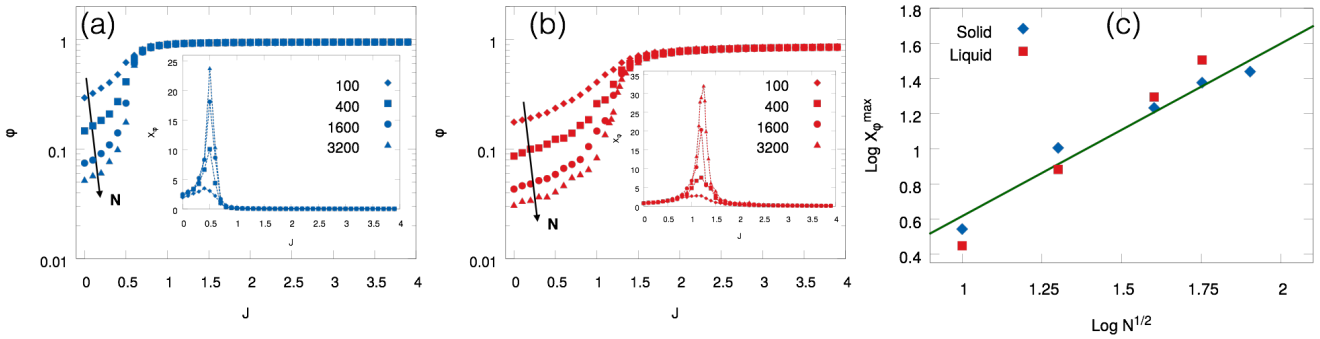

Fig. S1. Flocking transition. (a) Order parameter φ as a function of J in the solid phase ($p_0 = 3.0$) by increasing $N = 100, 400, 1600, 3200$. From φ we evaluate the fluctuations χ_φ (inset) that develops a peak at the transition. (a) Order parameter φ as a function of J in the liquid phase ($p_0 = 3.7$) by increasing $N = 100, 400, 1600, 3200$ and susceptibility χ_φ (inset). (c) The susceptibility χ_φ evaluated at the transition point as a function of the linear size $\sqrt{N}$ of the system.

To investigate the nature of the flocking transition, we have performed $N_J = 40$ numerical simulations from $J = 0$ to $J = 3.9$ at interval $\Delta J = 0.1$ at $p_0 = 3.0$, where the system is a jamming solid. In the liquid phase, we choose $p_0 = 3.7$ and $N_J = 48$. In particular, we performed 40 simulations with $\Delta J = 0.1$ and 8 simulations, close to the transition point J_c, with $\Delta J = 0.05$. The system sizes are $N = 100, 400, 1600, 3200$.

The typical behavior of the order parameter φ is shown in Fig. S1(a) and S1(b), for the solid and liquid, respectively. φ increases continuously from φ_{min} to φ_{max} following a sigmoidal curve. The extreme values φ_{min} are extremely size dependent and tends to zero by increasing the size N. The transition point J_c has been evaluated looking at the susceptibility $\chi_\varphi = N\langle(\varphi - \langle\varphi\rangle)^2\rangle$. As one can appreciate in the inset of the same panels, χ_φ develops a peak at J_c. In the solid, the peak occurs at $J_c^{solid} = D_r$. In the liquid, the transition takes place at $J_c^{liquid} > J_c^{solid}$. Moreover, the plateau values $\varphi_{max}^{liquid,solid}$ do not depend on the system size. In the liquid we obtain systematically $\varphi_{max}^{liquid} < \varphi_{max}^{solid}$ with $\varphi_{max}^{solid} \to 1$ and $\varphi_{max}^{liquid} \sim 0.8$. In Fig. S1(c) we show the values of χ_φ at the transition as a function of the linear size of the system $L = \sqrt{N}$. The behavior of the peak is well reproduced by a power law $\chi_\varphi(L) \sim L^b$ with $b \sim 1$ for both data sets, solid and liquid phases.

4. Neighbors mean-square separation

The estimate of the transition curve $J_{flock}(p_0)$ presented in the main text is based on the numerical computation of the cage lifetime τ_{cage} associated with the neighbors mean-square separation $MSS_{nn}(t)$, evaluated for $J = 0$. The neighbors mean-square separation is defined as:

$$MSS_{nn}(t) = \frac{1}{2N} \langle \sum_i \sum_{j(i)} [\mathbf{r}_i(t + t_0) - \mathbf{r}_j(t + t_0)]^2 \rangle , \quad [12]$$

where the sum is performed over all cells i and over the two cells $j(i)$ that, at time $t = t_0$, are the third and the fourth nearest neighbors of cell i, respectively. This choice is motivated by the following observation. Each cell i is on average in contact with six neighbors that constitute its "cage". Let d_{cage} be the average distance between cell i and its neighbors. At a given time, the first three nearest neighbors are typically closer to cell i than d_{cage} and thus their distance to cell i will tend to increase, at least for short times. On the contrary, higher order neighbors on average will move toward cell i. The third and the fourth nearest neighbors are those for which these systematic effects are expected to be less important. For example, in the solid phase, with our definition we find $MSS_{nn}(t) \approx$ const, for all t. A different definition, based for example on the first and the second nearest neighbors, would, on the contrary, show an increase at short times, followed by damped oscillation about an asymptotic value.

Our definition has the advantage of providing an indicator that is relatively insensitive to the intra-cage dynamics, allowing us to identify unambiguously the moment when two cells, initially in contact, start moving apart from each other, "breaking

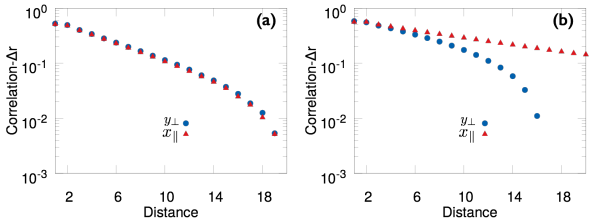

Fig. S2. Spatial correlations $C(x_\parallel, 0)$ (red triangles) and $C(0, x_\perp)$ (blue circles) along axes longitudinal ($x_\parallel$) and perpendicular ($x_\perp$) to the direction of mean motion of a given sample for $J = 0$ (a) and $J = 2$ (b), averaged over 10^2 samples.

the cage". Operatively, the cage timelife τ_{cage} is estimated as the time needed to double the neighbors mean-square separation with respect to its value at $t = 0$,

$$MSS_{nn}(\tau_{cage}) \equiv 2MSS_{nn}(0) \ . \qquad [13]$$

5. Correlation function of cell displacements

To quantify the dynamical heterogeneities and highlight their anisotropic structure in the flocking state, we have evaluated the spatial correlation of cell displacements $C(x_\parallel, x_\perp)$ along directions longitudinal ($x_\parallel$) and transverse ($x_\perp$) to that of mean motion.

We first calculate a coarse-grained map $\Delta\mathbf{r}(x, y)$ of cell displacements during a time interval $\tau_\alpha = 10^2$ on a lattice (x, y) of linear size $\delta_\ell = \sqrt{A_0}$. For a given realization we calculate the spatial correlation,

$$c(x, y) = \frac{\sum_{x',y'} \Delta\mathbf{r}(x + x', y + y') \cdot \Delta\mathbf{r}(x', y')}{\sum_{x',y'} |\Delta\mathbf{r}(x', y')|^2} \ . \qquad [14]$$

$C(x_\parallel, x_\perp)$ is obtained by averaging c over 10^2 independent realizations. The average is performed after rotating the axes by the angle θ identifying the average direction of migration in each sample:,

$$C(x_\parallel, x_\perp) = \left\langle c(x_\parallel \cos\theta - x_\perp \sin\theta, x_\perp \cos\theta + x_\parallel \sin\theta) \right\rangle \ . \qquad [15]$$

As one can appreciate in Fig. (S2), in absence of alignment ($J = 0$, panel (a)), the correlation is isotropic, but becomes strongly anisotropic in the flocking state ($J = 2$, panel (b)).

6. Dynamic and Static Structure of flocking state

In order to investigate the structural and dynamical properties of the flocking state, we have looked at the configurations and trajectories along the mean velocity.

The positional order has been investigated through the pair distribution function $g(\mathbf{r})$, where the vector $\mathbf{r}$ is computed in a moving frame orientated along the instantaneous flocking direction

$$g(\mathbf{r}) = \left\langle \frac{1}{N} \sum_{i,j\neq i} \delta(\mathbf{r} - \mathbf{r}_j + \mathbf{r}_j) \right\rangle \ . \qquad [16]$$

To estimate the asymmetry of the trajectories in the flocking state, we have computed the mean square displacement along the mean motion directions $x_\parallel$ and $x_\perp$. Since we are computing a dynamical observable, in this case the mean motions direction are defined over a time scale T_{flock}. The time scale T_{flcok} has been chosen in a way such that the flocking direction remain constant, i. e., $\frac{d}{dt}x_\parallel(t) = \frac{d}{dt}x_\perp(t) \sim 0$, for $t \in [t_0 + T_{flock}, t_0 + T_{flock}]$, being t_0 an arbitrary initial time. In Fig. (S3) we show $g(\mathbf{r})$ in the liquid phase ($p_0 = 3.7$) for $J = 0$ (lower panel) and in the flocking state with $J = 3.0$ (upper panel). As one can see, the system in the flocking state is an anistotropic fluid more dense along the flocking direction (blue curve).

Indicating with $x^i_\parallel(t)$ and $x^i_\perp(t)$ the coordinates of the cell i with respect the two orthogonal axes, we compute the mean square displacement $MSD(t)_\parallel$ and $MSD(t)_\perp$ as follows

$$\begin{aligned} MSD_\parallel(t) &= \frac{1}{N}\langle \sum_i [x_\parallel(t + t_0) - x_\parallel(t_0)]^2 \rangle \\ MSD_\perp(t) &= \frac{1}{N}\langle \sum_i [x_\perp(t + t_0) - x_\perp(t_0)]^2 \rangle \end{aligned} \qquad [17]$$

we then define the anisotropy parameter

$$\Delta \equiv \frac{MSD_\perp(T_{flock}) - MSD_\parallel(T_{flock})}{MSD_\perp(T_{flock}) + MSD_\parallel(T_{flock})} \ . \qquad [18]$$

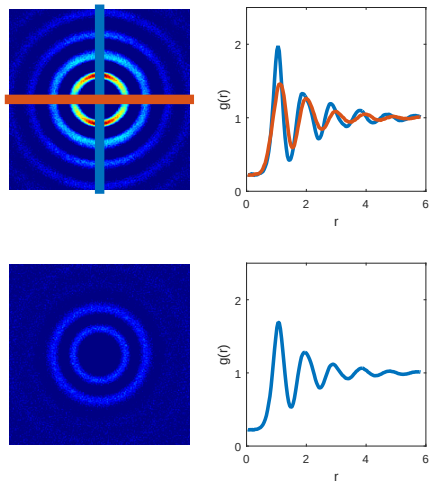

Fig. S3. Pair distribution function in the mean velocity frame.

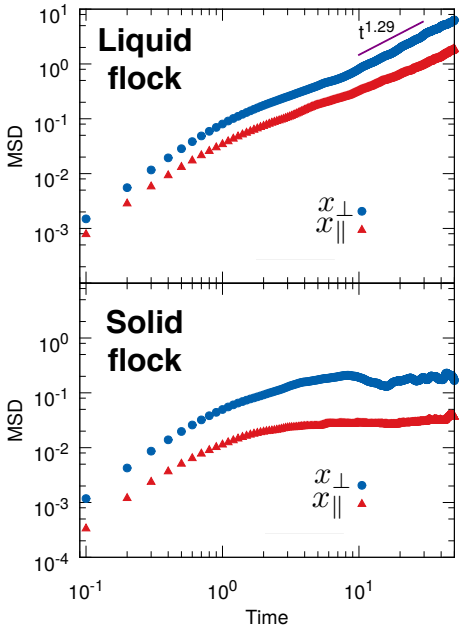

Fig. S4. Mean squared displacement in the mean velocity frame.

As one can appreciate in the upper panel of Fig. (S5) where the heat map $\Delta(p_0, J)$, the anisotropy parameter can be used as an order parameter for the flocking transition since it is zero when the system is in the solid and liquid phase. We have also included the transitions curve of the solid-to-liquid transition (red curve) and flocking transition (white dashed curve).

7. Computation of the cell shape

To investigate the coupling between cell morphology and flocking transition we start with computing the shape tensor S_i of the cell i that is

$$\mathbf{S}_i = \frac{1}{N_v} \sum_{\mu=1}^{N_v} (\mathbf{r}_i - \mathbf{r}_i^\mu) \otimes (\mathbf{r}_i - \mathbf{r}_i^\mu) \qquad [19]$$

where the greek symbol μ runs from 1 to the number of vertices N_v of the cell i, and $\mathbf{r}_i^\mu$ is the coordinate of the $\mu-$th vertex. We have indicated with $\otimes$ the standard dyadic product. In two dimensions, $\mathbf{S}_i$ is a 2×2 matrix of eigenvalues $\lambda_{1,2}$ and normalized eigenvectors $\hat{\boldsymbol{\lambda}}_{1,2}$. For convenience, we order the eigenvalues in a way that $\lambda_1 \geq \lambda_2$. When $\lambda_1 = \lambda_2$, the cell is a regular polygons and it is elongated along $\hat{\boldsymbol{\lambda}}_1$ whereas $\lambda_1 \neq \lambda_2$.

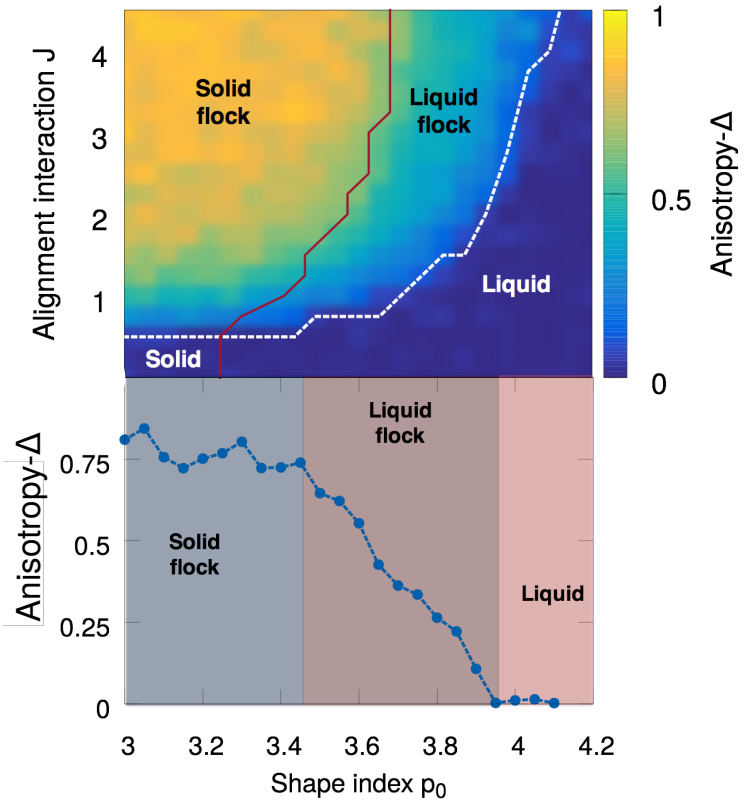

Fig. S5. Anisotropy Parameter. The anisotropy parameter can be used as an order parameter for the flocking transition (upper panel). For $J = 3.00$ (lower panel), Δ is zero in the liquid and becomes different from zero in the flocking state.

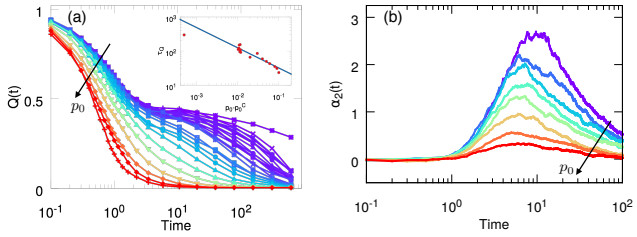

Fig. S6. Dynamical arrest and flocking transition. (a) The overlap $Q(t)$ for $J = 2.0$ shows a clear two step decay typical of glassy dynamics. From $Q(t)$ we can extract a correlation time τ_q (inset) that increases as a power law as a function of $p_0 - p_0^C$. (b) The non-Gaussian parameter $\alpha_2(t)$ develops a clear peak indicating the presence of angular dynamical heterogeneity in the flocking state.

8. Overlap and non-Gaussian parameter

To estimate the effect of alignment on structural rearrangements we have also looked at the behavior of the overlap parameter, $Q(t)$. The overlap gives a measure of the similarity between two configurations of the system taken at two different times, in our case at t and 0 (34, 35). To compute $Q(t)$, we discretize space in a lattice of linear size $\delta \sim 0.66$ and define $n_i(t, t_0) = 1$ if the site i s occupied by the same particle at time t_0 and $t > t_0$, and $n_i(t, t_0) = 0$ otherwise. The overlap is defined as

$$Q(t) = N_s^{-1} \langle \sum_i n_i(t, t_0) \rangle \ . \qquad [20]$$

Here N_s is number of lattice sites. In order to exclude fast vibrations on short time scales, we choose the parameter δ through the condition $\delta = \sqrt{MSD(t_{s-d})}$, where t_{s-d} is the crossover time from subdiffusive to diffusive regime. As one can appreciate looking at Fig. S6(a), where Q(t) for $J = 2.0$ is shown, the overlap undergoes a two-step decay typical of glassy systems indicating a crossover between fast and slow processes. Remarkably, the crossover takes place around the flocking transition indicating that the emergence of collective migration changes the structural properties. This is also highlight in the main text through the study of dynamical heterogeneities. In the inset of the same figure, we plot $\tau_Q \equiv \int_{t^*}^{\infty} dt\, Q(t)$, where t^* is chosen in a way to extract only the slow β decay of $Q(t)$. Interestingly, τ_Q can be fitted to a power law as a function of $p_0 - p_0^C$, which is compatible with mode-coupling theory (34).

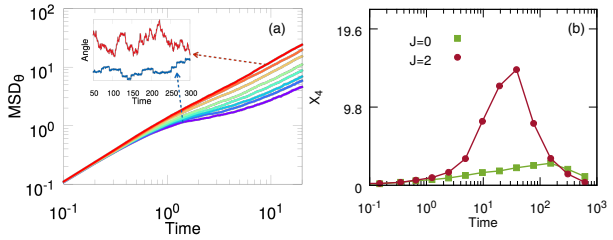

Fig. S7. Mean-squared angular displacement MSD_θ. (a) MSD_θ of the polarization angle θ for $J = 2.0$ and $p_0 \in [3.0, 3.5]$, i. e., in the flocking regime. MSD_θ becomes subdiffusive on short time scales. Also shown are two typical angular trajectories: for large p_0 (red curve) $\theta(t)$ performs a random walk while for small p_0 (blue curve) the dynamics of $\theta(t)$ is characterized by jumps local and vibrations. (b) $\chi_4(t)$ approaching the liquid-solid transition ($p_0 - p_0^c/p_0^c \sim 10^{-3}$) for $J = 0$ (green squares) and $J = 2$ (red circles) in a system of $N = 4900$ cells.

The time scale τ_Q is also compatible with the time scale of the peak in the non-Gaussian parameter of the angular displacements $\alpha_2(t) \equiv \frac{1}{3}\frac{\langle \Delta\theta^4 \rangle}{\langle \Delta\theta^2 \rangle^2} - 1$, where $\Delta\theta^a \equiv \sum_i N^{-1} [\theta_i(t + t_0) - \theta_i(t_0)]^a$. The behavior of $\alpha_2(t)$ is shown in Fig. S6(b). Also, since the time scale of angular relaxation is an order of magnitude smaller than that of structural relaxation, the displacements due to the flocking excitations give the dominant contribution to the displacements.

9. Videos

We have included representative movies illustrating the monolayer dynamics in four different phases for $N = 400$ cells.

- M1.avi - Representative portion (1000 simulation steps) of a simulation of the cell dynamics when the monolayer is in a solid phase. Simulation parameters are $p_0 = 3.0$ and $J = 0.0$. A small cluster of cells that are nearest neighbors at the beginning of the movie is represented in color. In the absence of local rearrangements and directed migration, the cluster remains cohesive and its center of mass does not show any net displacement.

- M2.avi - Representative portion (1000 simulation steps) of a simulation of the cell dynamics when the monolayer is in a liquid phase. Simulation parameters are $p_0 = 3.7$ and $J = 0.0$. A small cluster of cells that are nearest neighbors at the beginning of the movie is represented in color. The presence of local rearrangements can be clearly appreciated, while the center of mass of the cluster of tagged cells does not show any net displacement.

- M3.avi - Representative portion (1000 simulation steps) of a simulation of the cell dynamics when the monolayer is in a flocking liquid phase. Simulation parameters are $p_0 = 3.7$ and $J = 3.0$. A small cluster of cells that are nearest neighbors at the beginning of the movie is represented in color. The presence of local rearrangements, superimposed to a collective directed migration pattern, can be clearly appreciated.

- M4.avi - Representative portion (1000 simulation steps) of a simulation of the cell dynamics when the monolayer is in a solid phase. Simulation parameters are $p_0 = 3.0$ and $J = 3.0$. A small cluster of cells that are nearest neighbors at the beginning of the movie are represented in color. In the absence of local rearrangements, the collective directed migration pattern can be clearly appreciated.

We have also included representative movies illustrating the monolayer dynamics, as observed in the center of mass reference frame, in four different phases for $N = 400$ cells. This representation allows to capture the anisotropic nature of the positional fluctuations of the cell when the monolayer is in a flocking state.

- M1w.avi - Representative portion (1000 simulation steps) of a simulation of the cell dynamics, when the monolayer is in a solid phase. Simulation parameters are $p_0 = 3.0$ and $J = 0.0$. A 50 simulation steps-long trajectory is shown for each cell center (time is color-coded from red to green). The black arrow in center is proportional to the instantaneous velocity of the center of mass.

- M2w.avi - Representative portion (1000 simulation steps) of a simulation of the cell dynamics, when the monolayer is in a liquid phase. Simulation parameters are $p_0 = 3.7$ and $J = 0.0$. A 50 simulation steps-long trajectory is shown for each cell center (time is color-coded from red to green). The black arrow in center is proportional to the instantaneous velocity of the center of mass.

- M3w.avi - Representative portion (1000 simulation steps) of a simulation of the cell dynamics, when the monolayer is in a flocking liquid phase. Simulation parameters are $p_0 = 3.7$ and $J = 3.0$. A 50 simulation steps-long trajectory is shown for each cell center (time is color-coded from red to green). The black arrow in center is proportional to the instantaneous velocity of the center of mass. The marked anistropy in the cell positional fluctuations can be clearly appreciated.

- M4w.avi - Representative portion (1000 simulation steps) of a simulation of the cell dynamics, when the monolayer is in a flocking solid phase. Simulation parameters are $p_0 = 3.0$ and $J = 3.0$. A 50 simulation steps-long trajectory is shown for each cell center (time is color-coded from red to green). The black arrow in center is proportional to the instantaneous velocity of the center of mass. The marked anistropy in the cell positional fluctuations can be clearly appreciated.

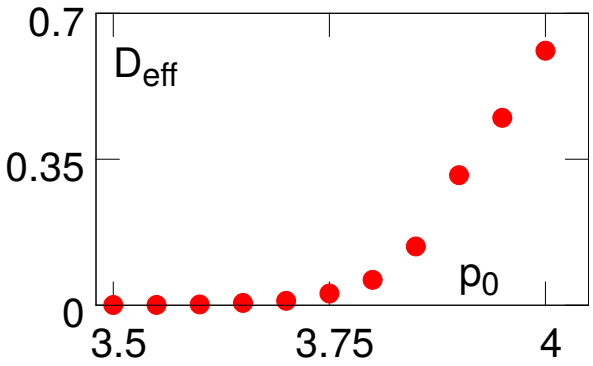

Fig. S8. Rigidity transition. Normalized self-diffusivity $D_{self} \equiv \lim_{t\to\infty} \frac{MSD(t)}{4tD_0}$ as a function of the shape index p_0 for $J = 2.0$. D_{self} is a dynamical order parameter for the onset of rigidity. When $D_{self} < 10^{-3}$ the system is considered to be in solid state.